Spontaneous Refolding of the Pore-Forming Colicin A Toxin upon Membrane Association As Studied by X-Band and W-Band High-Field Electron Paramagnetic Resonance Spectroscopy†

Anton Savitsky,‡ Martin Kühn,§ Denis Duché,|| Klaus Möbius,*,‡ and Heinz-Jürgen Steinhoff*,§

Fachbereich Physik, Freie Universität Berlin, Arnimalle 14, D-14195 Berlin, Germany, Fachbereich Physik, Universität Osnabrück, Barbarastrasse 7, D-49069 Osnabrück, Germany, and Laboratoire d'Ingéniérie des Systèmes Macromoléculaires, Institut de Biologie Structurale et Microbiologie, CNRS, 31 chemin Joseph Aiguier F-13402, Marseille Cedex 20, France

Received: August 12, 2003; In Final Form: February 3, 2004

The pore-forming bacterial toxins of the colicin family undergo massive protein refolding, while attacking a target cell, to convert from the water-soluble conformational state to the membrane-associated state with subsequent insertion of helical hairpins into the cytoplasmic membrane. To explore the validity of proposed models for the mechanism by which the soluble channel-forming domain of colicin A turns inside out upon membrane association, five site-specific cysteine mutants of colicin A, each singly spin labeled with nitroxide side chains, were studied by 9.5 GHz (X-band) and 95 GHz (W-band) high-field EPR. By elucidating the mobility of the nitroxide side chains on one of the two hydrophobic helices and their accessibility to paramagnetic relaxer molecules in the membrane, as well as by measuring the g_{xx} and A_{zz} nitroxide tensor components, detailed information about conformational changes upon membrane association could be revealed. This information on the channel-forming domain of colicin A goes beyond that available already from X-ray crystallography. The multifrequency EPR results are in favor of the "penknife" model of the membrane-associated channel-forming domain of colicin A with the ion channel still closed in the absence of additional modulation of the membrane potential. The results cannot exclude the existence of a thermodynamic equilibrium with other conformations in which the "penknife" state is predominantly populated.

Introduction

Pore-forming colicin A is a member of a family of plasmid encoded bacterial toxins that, different from most toxins, are toxic to their own bacterial host, but not to other species.[1] Colicins are produced by and toxic to *Escherichia (E.) coli*,[1,2] but their plasmid bears an immunity protein that ensures protection of the organism from the colicin toxin. Seven members of the ion-channel forming colicins are currently identified and sequenced, denoted E1, A, B, K, N, Ia, Ib.[1,3,4] They are water-soluble proteins, mostly about 60 kD in size, and have varying homology among themselves.

Colicin A kills unprotected cells of attacked organisms by inserting specific portions of protein subdomains into the cytoplasmic membrane forming a voltage-gated ion channel. The open channel leads to electrical depolarization of the membrane and depletion of intracellular ion pools, which ultimately leads to cell death. The mechanisms of protein entry into membranes and transmembrane channel formation are fundamental aspects of membrane biology and toxicology. To understand these mechanisms on the molecular level is currently also of biomedical interest, because insertion of proteins into membranes and subsequent channel formation are common to many toxic proteins of bacterial pathogens found in organisms ranging from bacteria to humans, such as the diphtheria, tetanus, and cholera toxins.[3−7]

The colicin toxins have to overcome the protecting barriers of the attacked cell and, hence, the mechanisms of cell killing involve three distinct functional steps:[1,8] binding of the toxic protein to a receptor at the surface of the outer membrane, translocation across the outer membrane and periplasm, and insertion of specific helical segments of the toxin subdomain into the cytoplasmic membrane to form the ion-conducting channel.

Accordingly, colicin A consists of three functional protein domains: the central receptor domain, R; the N-terminal translocation domain, T, to penetrate the outer membrane (aided by the receptor proteins Btu B and OmpF of the target cell)[2,4] and to traverse the periplasm (aided by several membrane translocation Tol proteins of the target);[2,4] and the C-terminal channel-forming domain, C, to penetrate the inner membrane that protects the cytoplasm of the cell.[2,4]

These distinct functions of the colicins are nicely reflected by their three-dimensional shape. The X-ray crystal structure of a complete (T−R−C) colicin Ia protein was recently determined to 3.0 D resolution,[9] now refined to 2.3 D,[4] and reveals a harpoon-shaped molecule, 210 D long, with the three functional domains well separated from each other. The long α-helices that link R with T and C enable the colicin molecule to span the periplasmic space and contact both the outer and inner membranes simultaneously during function,[9] thereby overcoming the protection barriers of the attacked cell.

For the toxic activity in vivo, all three domains, T, R, and C, are essential, but the isolated C-domain retains its channel-

† Part of the special issue "Jack H. Freed Festschrift".

* To whom correspondence should be addressed. E-mail: (K.M.) moebius@physik.fu-berlin.de, (H.-J.S.) heinz-juergen.steinhoff@uos.de.

‡ Freie Universität Berlin.

§ Universität Osnabrück.

|| Institut de Biologie Structurale et Microbiologie.

10.1021/jp036397l CCC: $27.50
Published on Web 04/02/2004

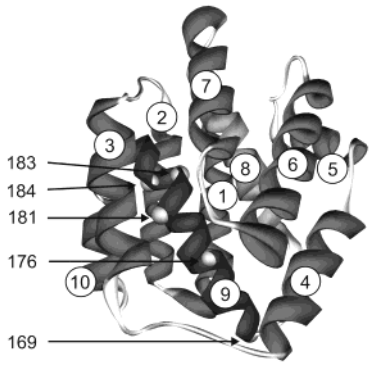

Figure 1. X-ray structure of the channel-forming C-domain of colicin A.[12] The positions of cysteine replacements by site-directed exchange mutagenesis[16,19] are indicated by numbered spheres. The α-helices are labeled 1 (N-terminus) to 10 (C-terminus). For details, see refs 16 and 19.

forming ability in aqueous solutions of artificial membranes,[10,11] such as lipid vesicles. Hence, details of the refolding processes of the C-domain that occur during the stepwise pore formation can be studied by in vitro experiments (see below).

The X-ray crystal structure of the 204-residue (21 kD) channel-forming polypeptide C of colicin A in its water-soluble conformation is available to 2.4 D resolution[12] (see Figure 1). Ten α-helices, eight amphiphilic and two hydrophobic ones, are arranged in such a way that the amphiphilic helices surround the hydrophobic hairpin (helices 8 and 9) deeply buried in the center of the protein. Thereby the 8, 9 hairpin is shielded from contact with the water solvent. The positively charged residues of the shielding helices are located at one end of the C molecule.

Despite the many years of experimental work on colicin A (and E1), the details of the refolding processes upon membrane association and channel formation as well as the structure of the transmembrane channel are not yet known. Because these colicins are now so well characterized, they may serve as a paradigm system to answer an intriguing question of general interest in molecular biology and medicine: What is the mechanism that provides energetically accepted pathways for insertion of water-soluble pore-forming proteins into the nonpolar lipid environment of a membrane?

In view of the difficulties encountered with crystallization of membrane proteins and with determining X-ray structures of transient states of proteins in action, numerous spectroscopic techniques are being used to study colicins on the molecular level. They allow us to follow up the individual steps of forming closed and open transmembrane channels and to elucidate the structure of these functional protein states in the polar and nonpolar regions of the phospholipid bilayer.[7] Prominent examples are solid-state NMR,[13,14] FT-IR,[15] and the use of site-directed cysteine mutagenesis to introduce fluorescent or nitroxide spin labels in conjunction with fluorescence resonance energy transfer (FRET)[16] or electron paramagnetic resonance (EPR) techniques.[8,17,18] These techniques are particularly powerful to test and refine current models of pore formation in biomembranes.

The C-domain of colicin A (and other members of the colicin family) can adopt two conformations, the water-soluble form and the transmembrane form. The transition between these conformations, which are energetically exclusive to each other, requires massive refolding of the tertiary structure. To date, two alternative models are being discussed to explain how the C-domain turns itself inside out to form the membrane-associated state with pore formation, the "umbrella" model[12] and the "penknife" model[16] (see Figure 2). Conceptually, they differ in the description of the relatively slow (100 ms to seconds range) membrane-insertion step to be either spontaneous or voltage dependent. Common to both models is the assumption that the rapid (several seconds) membrane association of the C-domain at sufficiently low pH values is due to Coulomb interaction between positively charged outer protein parts and the negatively charged membrane surface.

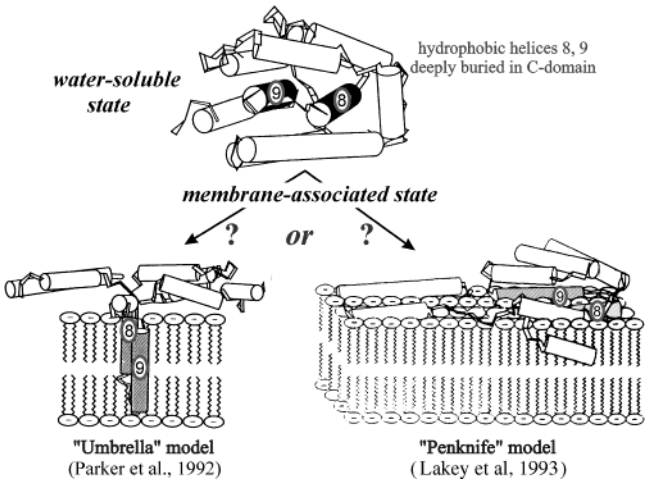

Figure 2. "Umbrella" model[12] and "penknife" model[16] of the membrane-associated state of the channel-forming C-domain of colicin A.

After docking to the membrane surface, a slow, still voltage-independent, refolding of the C-domain occurs to bring the hydrophobic helices 8 and 9 to the outside of the protein complex. In the umbrella model the hydrophobic hairpin 8, 9 spontaneously traverses the membrane, whereas in the penknife model the refolding leaves the 8, 9 hairpin close to the membrane surface, but a change of the electric transmembrane potential, $\Delta\Psi$, is required to trigger insertion of the 8, 9 hairpin into the membrane. The occurrence of a $\Delta\Psi$ signal also initiates insertion of amphiphilic helix hairpins of the C-domain. They make the membrane permeable for ion flow, i.e., open the channel.

For colicin A double-fluorescent-label FRET experiments have been performed to measure the interhelical distance in the membrane-associated state.[16] From these experiments the umbrella model was rejected because the postulated large distances between the hydrophobic hairpin and the remainder of the molecule were not observed.[16,19]

The situation might be different in the case of the homologous colicins E1 and Ia for which experimental evidence has been published that supports the umbrella model, i.e., the notion of spontaneous hydrophobic hairpin insertion into the membrane before a $\Delta\Psi$ signal enables insertion of additional helices.[8,20−22] Among these experiments on colicin E1 those of Hubbell and collaborators[8,17,18] are of particular interest in respect to our work on colicin A as they also used the approach of site-directed spin labeling (SDSL, for reviews see, for example, refs 23−26) in conjunction with EPR spectroscopy. These authors used conventional X-band (9.5 GHz) EPR as spectroscopic tool, whereas in our work also high-field EPR at 95 GHz was used to take advantage of the dramatically increased spectral resolution at high Zeeman fields (for reviews see, for example, refs 27−30).

In recent SDSL/high-field EPR work on NO• labeled proteins we have shown that, in addition to the A_{zz} hyperfine tensor component of the ^{14}N nucleus, also the g_{xx} tensor component can be used as sensitive probe for the polarity and proticity of

the microenvironment of the nitroxide side chain and for its motional characteristics in three-dimensional space under the local constraints of the protein.[31−33]

Additional information about orientation and local environment was obtained by measuring, via X-band EPR, the accessibility of the NO• spin label at the various protein positions to freely diffusing paramagnetic probe molecules (spin relaxers), such as molecular oxygen (O_2) and water-soluble chromium oxalate (CROX). Such accessibility experiments have proven to be ideally suited to identify the local environment as polar (water/membrane interface, where the collision frequency between CROX and NO• is high) or nonpolar (inner membrane, where the collision frequency between O_2 and NO• is high).[34−38] Collisions between the relaxer molecules and the NO• spin label lead to Heisenberg spin exchange with concomitant shortening of the electronic relaxation times proportional to the respective relaxer concentration in the interface and the interior of the membrane. Thus, from EPR measurements of the relaxation times of the site-specifically NO• labeled protein, for example, by saturation experiments, in the presence and absence of O_2 or CROX, information about the accessibility to the relaxer molecules and, hence, about the topography of the labeled protein segment in the membrane could be inferred. In the following it will be shown that both the X-band EPR accessibility experiments and the W-band EPR measurements of the g_{xx} and A_{zz} tensor components of the selectively labeled hydrophobic helix 9 of colicin A are in favor of the penknife model of the membrane-associated C-domain.

Experimental Section

Mutagenesis, Expression, and Spin Labeling. Mutagenesis, protein expression and purification were performed as described by Duché et al..[16,19] The following steps were performed at 4 °C. The protein samples were incubated with 10 mM dithioerythritol (DTT) for several hours. Prior to spin labeling the samples were washed by repeated dilution and concentration steps with sodium phosphate buffer, pH 6.8, using an *Amicon* ultra filtration unit (filters PM10 or YM2, Millipore, or RC/10, Schleicher&Schuell) to dilute the DTT concentration to less than 100 μM. For spin labeling with (1-oxyl-2,2,5,5-tetramethylpyrrolin-3-ylmethyl)methanethiosulfonate (MTSSL, side chain denoted R1) (TRC), 30 μL of a 100 mM MTSSL solution in acetonitrile was added to 3 mL of colicin (concentration 10−15 mg/mL) in 0.1 M phosphate buffer, pH 6.8, resulting in a spin label concentration of 1 mM. The samples were incubated for at least 1 h. To unfold the protein and provide efficient accessibility to the internally located cysteines, spin labeling of mutants G176C, A181C, and V183C was performed in the presence of 6.5 M guanidinium hydrochloride (GdnHCl). The noncovalently bound spin label and the GdnHCl were removed by repeated washing and a final dialysis against 10 L of 10 mM sodium phosphate buffer, pH 7.4. The spin labeled protein was concentrated to 10−15 mg/mL and stored at −80 °C.

The activity of the spin labeled mutants A169R1, G176R1, A181R1, and G184R1 was identical to that of the wild type protein, as determined by the minimum colicin concentration required to significantly inhibit bacterial growth. The activity of G184R1 was slightly reduced.

Colicin A was found to be unstable at acidic pH values but exhibits high stability around pH 8. Hence, all measurements were performed in buffered solutions at pH 8 providing physiological conditions. For EPR measurements in the absence of lipids 5 μL of the protein stock solution was diluted with 3 μL of a 100 mM sodium phosphate buffer, pH 8, and 4 μL of distilled water. For measurements in the presence of lipids 5 μL of the protein stock solution was diluted with 3 μL of a 100 mM sodium phosphate buffer, pH 8, and 4 μL of a stock solution of small unilamellar vesicles made by sonification of L-α-phosphatidyl-DL-glyceroldimyristoyl (DMPG, Sigma) in water (25 mg/mL). After 15 min incubation the samples were shock frozen in liquid nitrogen, thawed, and sonificated[39] in an ultrasonic bath (Bandelin-Sonorex). This procedure was repeated twice.

Accessibility and Mobility Measurements by X-Band EPR. X-band EPR measurements were performed on homemade equipments as described earlier.[37,38] The X band EPR spectrometer is equipped with a H_{103} cavity (AEG), a dielectric resonator ER4118X-MD5 (Bruker) or a homemade loop-gap resonator.[40] The B−NM 12 gaussmeter (Bruker) was used to measure the magnetic field. The colicin samples were loaded into EPR quartz capillaries (3 mm i.d., 50 μL for low-temperature measurements, 0.9 mm i.d., 10 μL for room-temperature measurements). The spectra were recorded with a modulation amplitude of 0.2 mT (T = 170 K) or 0.15 mT (T = 296 K). After analog-to-12-bit digital conversion, the data were processed in a personal computer.

The accessibilities for paramagnetic quenchers were quantified by the method of continuous wave (cw) power saturation.[36,41] The protein samples were loaded into gas-permeable TPX capillaries (Spintec). The samples were deoxygenated by a nitrogen gas flow around the sample capillary. For oxygen accessibility experiments, nitrogen was replaced by air or pure oxygen. Saturation curves were determined from the first derivative peak-peak amplitudes of the center line, A', measured at different incident microwave power levels in the range from 0.1 to 70 mW and fit to the power saturation equation

$$A'(P) = I\frac{\sqrt{P}}{(1 + \sigma\alpha^2 P)^{\epsilon}} \qquad (1)$$

where P is the microwave power incident on the sample, α is the conversion efficiency factor of the resonator, I is a scaling factor, and σ is the saturation parameter which depends on the longitudinal and transversal relaxation times, T_1 and T_2, of the sample: $\sigma = \gamma^2 T_1 T_2$. During the fit, the scaling factor I and the product $\sigma\alpha^2$ are adjustable parameters. The measure of the homogeneity, ϵ, is 3/2 for a homogeneous line and 1/2 for a completely inhomogeneous line shape. During the fit, this parameter accounts for inhomogeneous broadening due to the restricted slow dynamics of the nitroxide. The strength of the microwave B_1 field along the sample in the dielectric resonator is not constant but leads to an inhomogeneous saturation. This is also accounted for by the value of ϵ. In the case of very small relaxation times the uncertainty of this parameter increases and error bars of $\sigma\alpha^2$ were determined by fixing ϵ to lower and upper limits of 0.85 and 1.2 during each fit.[42] Multiplying $\sigma\alpha^2$ by the line width of the center line, $\Delta B_{pp} \propto T_2^{-1}$, yields a measure of T_1. In the presence of a relaxing agent T_1 is decreased according to $T_1^{-1} = T_{1(0)}^{-1} + \omega f$, where $T_{1(0)}$ is the relaxation time in the absence of the relaxer, ω is the collision frequency between the nitroxide and the relaxing agent, and f is a statistical factor. The difference in $(\sigma\alpha^2\Delta B_{pp})^{-1}$ values in the presence and absence of the relaxing agent is normalized by the same quantity of a Fremy's salt standard sample in 50 mM potassium carbonate to obtain a dimensionless accessibility parameter Π. This is proportional to the collision frequency, ω, of the nitroxide with the respective paramagnetic reagent.

High−Field EPR Measurements. The laboratory-built W-band high-field EPR spectrometer at FU Berlin operates in both

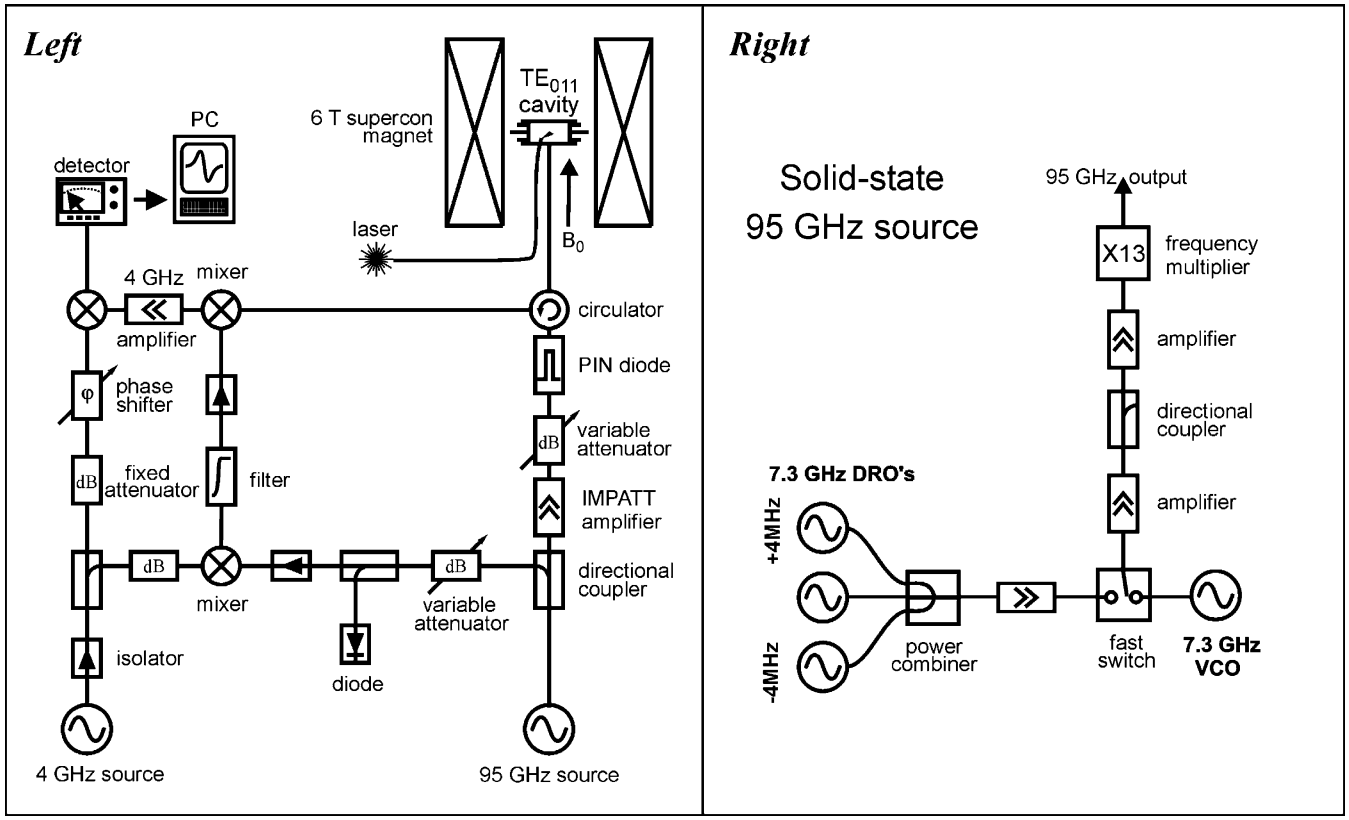

Figure 3. Block diagram of the laboratory-built 95 GHz high-field EPR spectrometer at FU Berlin.[43,44] Left: design of the heterodyne microwave bridge.[43] Right: configuration of the solid-state 95 GHz source.[44]

cw and pulsed mode at an EPR transition frequency around 95 GHz (3 mm wavelength) and an external magnetic field of about 3.4 T for $g = 2$ systems. Figure 3 (left and right) shows the block diagram of the spectrometer used in the present experiments:[43,44] left, the design of the heterodyne microwave bridge,[43] right, the configuration of the novel solid-state 95 GHz source.[44]

A superconducting cryomagnet (Cryomagnetic, max. $B_0 = 6$ T, room-temperature bore diameter 114 mm) provides the static magnetic field, which can be swept by ± 0.1 T by controlling the current in additional superconducting sweep coils inside the magnet Dewar. The field-modulation coils for cw EPR experiments are part of the probehead and supply up to 1 mT at the sample at about 10 kHz. Optional light excitation of the sample is achieved by a Nd:YAG laser (Spectra Physics) or a halogen lamp focused on a quartz-fiber light guide to the cavity.

The heterodyne microwave (mw) bridge works at an intermediate frequency (IF) of 4 GHz provided from the dielectric-resonator oscillator (DRO). The 4 GHz branch allows convenient manipulation of phase and amplification. The 99 GHz local-oscillator signal is obtained by up-converting the output power of the 95 GHz source (a klystron or a solid-state oscillator; see below) with that of the 4 GHz DRO. The 4 GHz power, resulting from down-conversion of the 99 GHz local-oscillator power and the power reflected from the EPR cavity, is amplified with a low-noise preamplifier and then down-mixed with the same 4-GHz DRO as local oscillator. The resulting signal is guided either to a lock-in amplifier or, after optional further amplification, to a fast digitizing scope (Tektronix). For more details, see ref 43.

Because of deteriorating performance of the klystron (Varian)-in the course of this work, it had to be replaced by a solid-state oscillator source (Elva-1). It uses four low-frequency oscillators, three fixed-frequency free-running, but temperature-stabilized, DRO's, and one voltage-controlled oscillator (VCO), operating at 7.3 GHz. The frequency of this mw field is further up-converted by a factor of 13 using an IMPATT-active frequency multiplier. An additional gain of the 95 GHz power is obtained by a two-stage cw IMPATT amplifier in the transmitter channel. The output power on the circulator of maximal +18.5 dBm (70 mW) allows us to perform pulsed EPR experiments with B/2 pulse lengths below 30 ns for the TE_{011} cavity. Also the cw EPR performance improved due to the outstanding frequency stability (below 30 kHz/h) and noise characteristics of the solid-state source (the amplitude noise is below −140 dBc/Hz at 10 kHz; the phase noise is below −100 dBc/Hz at 10 kHz).[44]

For the high-field EPR experiments the sample solutions (see methods) were transformed into quartz capillaries of 0.6 mm i.d. fitting to the frequency-tuning plungers of the TE_{011} cavity.[45] Owing to the low protein concentration achievable for the colicin A samples, five to eight spectra had to be accumulated for sufficient signal-to-noise ratio.

These problems with the S/N ratio were in contrast to our previous experience with SDSL/high-field EPR on, for instance, bacteriorhodopsin.[31,32] In this case, centrifugation of the sample capillary could be done to increase the protein concentration by approximately 1 order of magnitude. The colicin A samples, however, cannot be concentrated above 10−15 mg/mL to avoid precipitation. Moreover, addition of glycerol to the aqueous solution, to decrease dielectric losses of the sample, is biochemically detrimental.

Results and Discussion

The X-ray structure of the channel-forming C-domain of colicin A[12] with its 10 α-helices is shown in Figure 1. By numbered spheres the individual amino acid residues are indicated, which have been replaced by cysteines by means of exchange mutagenesis.[16,19] We started our studies with these

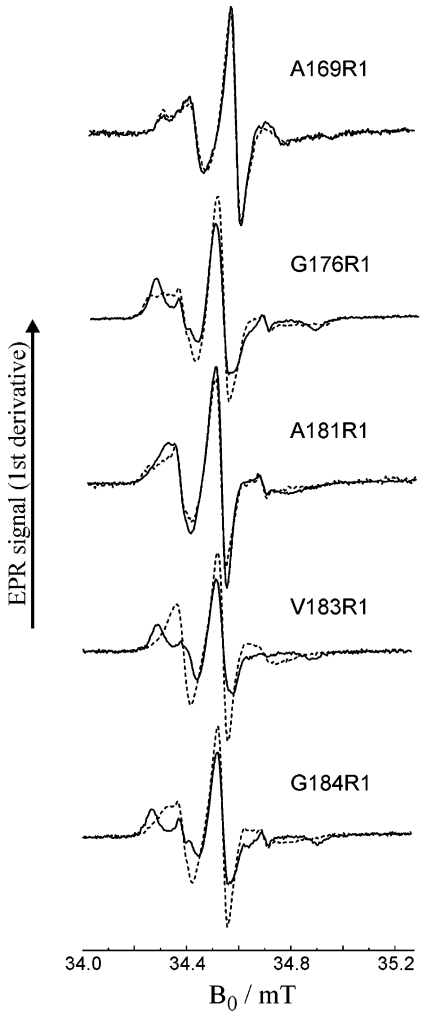

Figure 4. First-derivative EPR spectra (X-band) of colicin A cysteine mutants in aqueous solution, pH 8 (continuous lines), with the MTS spin label (side chain R1) bound to selected sites of helix 9 (cf. Figure 1). After addition of DMPG lipid vesicles (dashed lines), the mobility of the nitroxides at positions 176, 183, and 184 is significantly increased. The spectra of A169R1 and A181R1 disclose only minor alterations.

five colicin A mutants, which were generated by exchange of native amino acids in the hydrophobic helix 9 by cysteines at residue positions 169, 176, 181, 183, and 184. The single cysteines were spin labeled with the nitroxide spin label MTSSL, as described in the methods section.

The shape of the X-band EPR spectra measured at room temperature (Figure 4) reveal the restriction of the nitroxide residual mobility, which depends on the protein structure in the vicinity of the spin label binding site.[46,47] Comparably small apparent hyperfine splittings and small line widths of the center line were found for the spin-label side chains A169R1 and A181R1, the spectrum of A169R1 revealing two components. A169R1 is located at the end of helix 9 close to the loop region, which connects helices 8 and 9. In loop regions and helix termini the interaction of the spin-label side chain with neighboring side chains and backbone atoms has been shown to be small, thus the reorientational motion of the nitroxide is hardly restricted. Additionally, loops and helix termini show a considerable degree of flexibility, which may contribute to the observed side-chain dynamics. Consequently, the line width and the hyperfine splitting are small due to partial averaging of anisotropic components. The nitroxide side chain bound to position 181 in helix 9 is oriented toward the surface of the protein. It is located in a cleft formed by helices 3 and 10 allowing for residual motion of the $NO^{\bullet}$ side chain. The spectra of the nitroxides bound to positions 176, 183, and 184 exhibit strong motional restrictions, in agreement with their location in the interior of the protein, the spectral shapes resemble those of powder spectra.

TABLE 1: Accessibility of the Nitroxide Side Chains for Molecular Oxygen and Chromium Oxalate in the Absence and Presence of DMPG Vesicles

	A169R1	G176R1	A181R1	V183R1	G184R1
Π_{CROX}	1.4 ± 0.6	0.0 ± 0.1	0.1 ± 0.1	0.0 ± 0.1	0.1 ± 0.1
Π_{oxygen}	2.4 ± 0.9	0.2 ± 0.1	0.6 ± 0.3	0.2 ± 0.2	0.6 ± 0.3
$\Pi_{CROX, DMPG}$	0.1 ± 0.2	0.0 ± 0.1	0.0 ± 0.1	0.1 ± 0.1	0.0 ± 0.1
$\Pi_{oxygen, DMPG}$	1.5 ± 0.6	1.0 ± 0.4	2.0 ± 0.7	2.1 ± 0.8	1.5 ± 0.6

[a] Values of the accessibility parameter Π were determined according to eq 1 in the presence of oxygen, Π_{oxygen}, or in 10 mM chromium oxalate solution, Π_{CROX}, in the absence and presence of DMPG vesicles. The maximum error range was determined by fits with the parameter ϵ fixed to lower and upper limits of 0.85 and 1.2, respectively. A solution of Fremy's salt in 50 mM potassium carbonate, saturated with air, was used as a reference sample (see text).

In the presence of DMPG vesicles (dashed lines) the spectrum of A169R1 is indistinguishable from that determined in the absence of DMPG, the spectrum of A181R1 exhibits only small changes. However, the mobility of the $NO^{\bullet}$ side chains at positions 176, 183, and 184 significantly increases after addition of DMPG vesicles. Because these sites are deeply buried in the interior of the water-soluble conformation, the interaction of colicin A with the lipid must have lead to an opening of the C domain protein structure.

The study of the lipid-induced conformational change of the spin-labeled colicin A was supplemented by measuring the collision frequency of the nitroxide side chain with freely diffusing paramagnetic probe molecules. The collision frequency of such a probe with the $NO^{\bullet}$ side chain depends on the product of its translational diffusion coefficient and its local concentration. Molecular oxygen and the water-soluble chromium oxalate (CROX) have been frequently used and found to be ideally suited for these experiments because of their sizes and solubility properties[34,35,37]. CROX relaxer molecules cannot penetrate into the tightly packed interior of a protein, whereas both the solubility and diffusion coefficients of CROX are high in water. Therefore, the collision frequency between CROX and a spin-label side chain, which is exposed to the aqueous phase, is high. On the other hand, the collision frequency should approach zero for spin labels located in the interior of a protein. The application of cw power saturation[34] yields an accessibility parameter, Π, which is proportional to the collision frequency of the nitroxide with the paramagnetic reagent. The values determined in the absence and presence of DMPG vesicles according to the method described in refs 37 and 38 are given in Table 1.

In the absence of lipid, A169R1 is the only residue that reveals considerable accessibility to CROX and molecular oxygen. Hence, A169R1 faces the aqueous phase, in agreement with the colicin A structure. Within experimental error the values of Π_{CROX} are equal to zero for the other R1 side chains and their values of Π_{oxygen} are low. Hence, the nitroxide side chains attached to these positions are shielded from the aqueous phase and are only barely accessible for oxygen, due to the tight helix packing in the vicinity of the nitroxide binding site. Again, these findings are in agreement with the structural data determined for the wild-type protein.

In the presence of DMPG vesicles large changes of the accessibility parameters are observed for all samples. A169R1 becomes shielded from the aqueous phase, as is revealed by

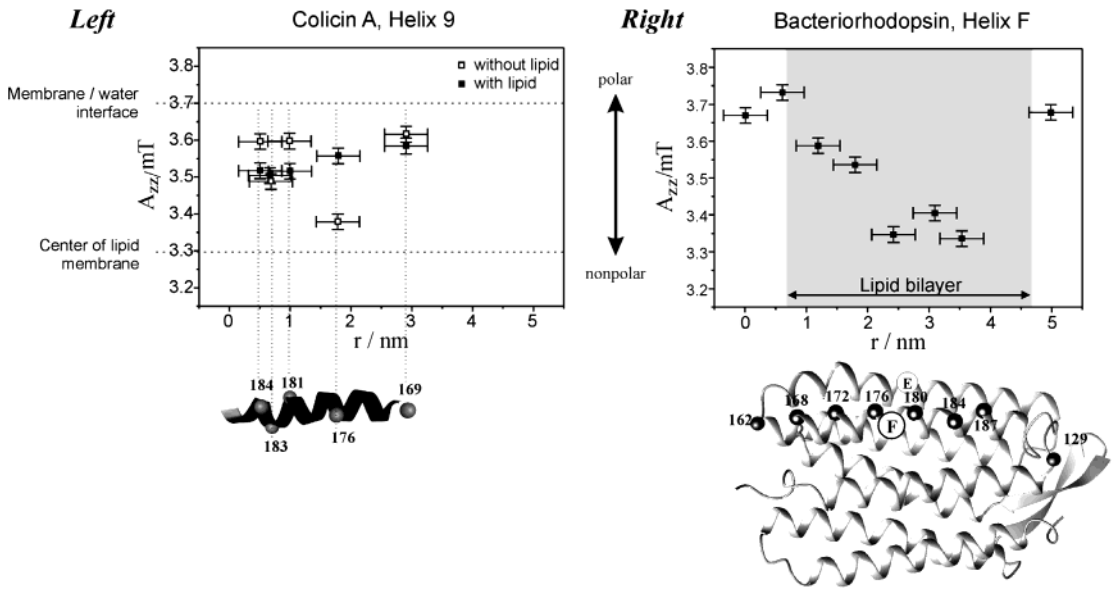

Figure 5. Left: X-band measurements of A_{zz} vs helix length as an index of the polarity in the nitroxide microenvironment for spin-label side chains in colicin A in aqueous solution without lipid (open squares) and in the presence of lipid vesicles (closed squares). Right: Comparison with the behavior of A_{zz} of nitroxides attached to the surface of the membrane-spanning helix F of bacteriorhodopsin (BR) revealing that helix 9 of colicin A penetrates less than 1.0 nm into the membrane. The coordinates of the amino acid positions of helix 9 in colicin A[12] and helix F in BR[58] are taken from the respective X-ray structures.

the decrease of Π_{CROX} by 1 order of magnitude. Low values of Π_{CROX} for all other mutants show that the NO• side chains are still not accessible from the aqueous phase. However, the oxygen accessibility is significantly increased by up to 1 order of magnitude. These results again imply an opening of the protein structure that exposes the nitroxide side chains to the protein surface. This surface is not accessible from the aqueous phase, as deduced from the low values of Π_{CROX}, but must be oriented to the lipid phase, as revealed by the high values of Π_{oxygen}.

To learn about the membrane-insertion mechanism leading either to a transmembrane configuration (as predicted by the umbrella model) or to a configuration with the hydrophobic helix 9 staying close to the water/membrane interface (as predicted by the penknife model), the ^{14}N hyperfine tensor components A_{zz} were measured for the five mutants. A_{zz} has proven to be a sensitive probe of the polarity profile of the NO• microenvironment along a helix structure.[31−33,38]

Figure 5 (left) shows A_{zz} (as deduced from X-band EPR) as a function of the length of helix 9 in colicin A in comparison with the membrane-spanning helix F (right) in bacteriorhodopsin (BR) determined as described by Steinhoff et al.[38] For colicin A, two situations are distinguished: aqueous solution (open squares), and aqueous solution in the presence of lipid vesicles (full squares). In the water-soluble conformation (no lipid added) the A_{zz} values reveal high polarity at both ends of helix 9, and a lower polarity in the center. This finding is consistent with the X-ray crystal structure.[12] After addition of lipid a rather uniform, high-polarity character of the nitroxide microenvironment of all mutants results. The highest polarity change is experienced by the NO• side chain attached to position 176 in the central part of the helix. In comparison, the respective A_{zz} data, determined for spin-label side chains attached to the outer surface of helix F of the transmembrane BR protein, shows a hydrophobic barrier. Such a hydrophobic barrier does not exist for the membrane-associated configuration of helix 9 of colicin A; i.e., this helix does not span the membrane. Moreover, the changes of A_{zz} upon addition of lipid reveal that all segments of helix 9 penetrate less than 1.0 nm into the artificial membrane.

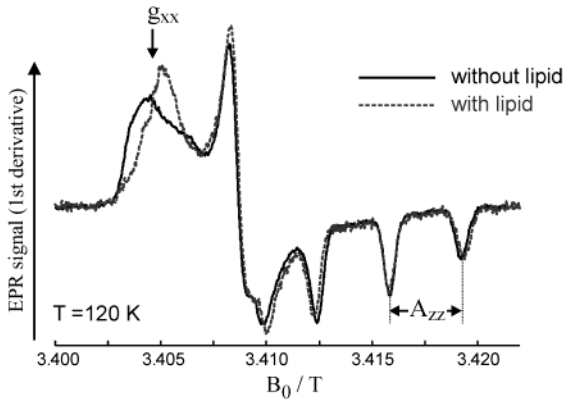

Figure 6. W-band EPR spectra of the colicin A mutant G176C with the NO• spin-label at position 176. The aqueous-solution and membrane-associated (with lipid) states show different g_{xx} and A_{zz} values. Artificial membranes are formed by adding an aqueous suspension (pH 8) of DMPG phospholipid vesicles (25 mg/mL). For details, see text.

To characterize the membrane contact of helix 9 in more detail, we performed W-band EPR experiments on frozen solutions (120−150 K) to determine both g_{xx} and A_{zz} as a measure of the polarity and proticity of the nitroxide microenvironment.[31−33] Despite the difficulties for sample preparations with appropriate colicin concentration, as compared to BR preparations (see above), and the accompanying signal-to-noise problems, we succeeded in obtaining W-band spectra of reasonable quality of colicin A mutants in their water-soluble state (without lipid admixture) and membrane-associated state (in phospholipid vesicles). Figure 6 shows, as a representative example, W-band spectra with and without lipid admixture of the colicin A mutant G176C. The spectra clearly reveal shifts of the g_{xx} and A_{zz} tensor components at the low-field and high-field regions, respectively. The S/N ration is good enough to extract reliable shift values of the tensor components upon lipid addition.

In Figure 7 the W-band measurements of g_{xx} and A_{zz} are summarized. Both probes show that the central-region position 176 experiences a strong change in polarity of the microenvi-

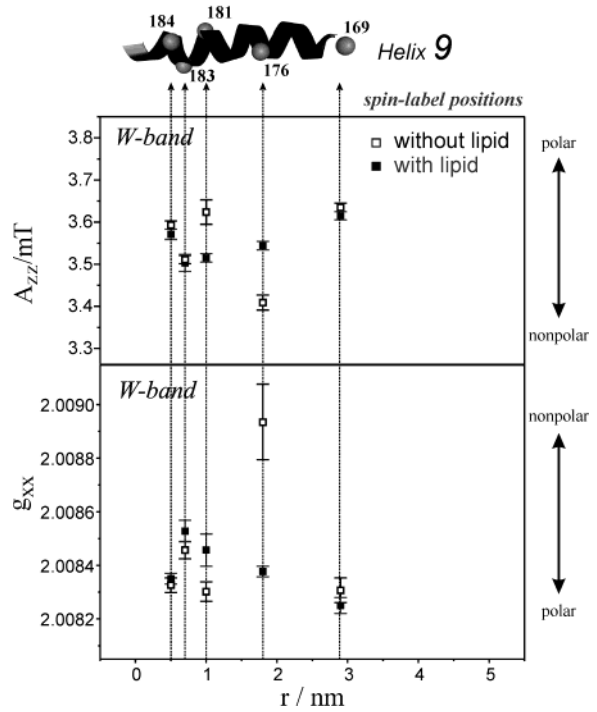

Figure 7. W-band EPR measurements of A_{zz} and g_{xx} tensor components vs length of helix 9 in colicin A. Top: A_{zz} shifts upon addition of lipid vesicles (closed squares), the A_{zz} values without lipid addition are marked by open squares. Bottom: g_{xx} shifts upon addition of lipid vesicles (closed squares), the g_{xx} values without lipid addition are marked by open squares. The coordinates of helix 9 in colicin A are taken from the X-ray structure of the water-soluble channel-forming C-domain.[12]

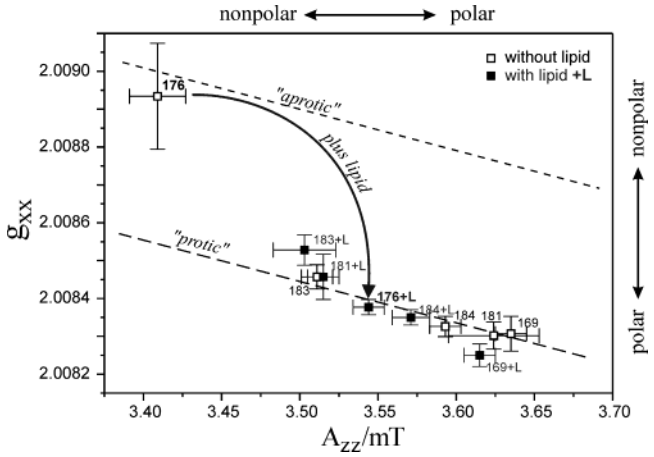

Figure 8. Polarity plot of g_{xx} vs A_{zz} for the various nitroxide spin-label positions in helix 9 of site-directed colicin A mutants. The measured tensor components with addition of lipid vesicles and without lipid addition are marked by full and open squares, respectively. The error bars are estimated from the S/N ratio of the W-band spectra, which is different for the various mutant samples (see text). The dashed lines define the limits between the non-hydrogen bonded "aprotic" (short dashes) and the fully hydrogen bonded "protic" (long dashes) cases, as previously reported.[33]

ronment toward more polar character, whereas in the vicinity of the end-region positions 169 and 184 only weak polarity changes occur upon adding lipids. This different behavior of polarity changes upon membrane association for position 176 and positions 169 and 184 is especially evident from the plot g_{xx} vs A_{zz} (see Figure 8). Such plots have proven to be highly informative about local electric-field and hydrogen-bonding effects of the microenvironments on the NO• spin labels. They allow conclusions to be drawn about dominant contributions to effects of the electronic structure of the nitroxide due to polarity changes or hydrogen bonding.[31−33,48−54] As is shown in Figure 8, addition of DMPG lipid results in a dramatic change of the microenvironment in the vicinity of position 176 toward an increased polarity.

How can these X- and W-band EPR results be rationalized in terms of the validity of either the umbrella or the penknife model of the membrane-associated configuration of the colicin A channel-forming C-domain? As stated above, in the water-soluble state, the two hydrophobic helices 8 and 9 are buried inside the domain, where they are energetically stabilized on a nonpolar microenvironment. In the membrane-associated state, the C-domain refolds to relocate the two hydrophobic helices on the surface of the domain.

For the umbrella model, helices 8 and 9 penetrate spontaneously the membrane so that their central part, as probed by the nitroxide side chain 176 in helix 9, would be placed into the membrane's interior, i.e., in a highly nonpolar region. This means that in the umbrella model one would expect for spin label 176 no large changes of g_{xx} and A_{zz} upon adding lipid to the aqueous sample because in both states, water-soluble and membrane-associated, the microenvironment would remain nonpolar.

For the penknife model, on the other hand, helix 9 remains for some time in a transient state close to the membrane surface—until an electric potential change $\Delta\Psi$ initiates helix insertion and pore formation in the membrane. In this situation, position 176 would experience a drastic change of the microenvironment from nonpolar to polar in the membrane-associated state.

This is exactly what we observe by means of the polarity probes g_{xx} and A_{zz} when adding vesicle-forming lipids to the aqueous sample. Hence, our data are not consistent with the umbrella model but validate the penknife model for membrane association of the colicin A channel-forming domain. The questioning of the umbrella model is in agreement with FRET experiments on colicin A double mutants with site-specifically attached fluorescence labels, for which the large interhelical distances required for the umbrella model were not measured.[16]

Our results do not exclude the existence of yet another conformation of colicin A for the closed channel state. For colicin E1 and colicin Ia Tory et al.[55] and Kienker et al.[56] suggested a thermodynamic equilibrium between two conformations according to the umbrella and the penknife model. For colicin E1 this equilibrium is shifted toward the umbrella model, whereas for colicin Ia a conformation according to the penknife model is predominantly populated. The equilibrium may significantly depend on the colicin type, the composition of the membrane and the pH value.[56] The influence of these parameters on the conformation of colicin A remains to be elucidated.

Outlook

In continuation of the described work on helix 9 mutants of colicin A, analogous multifrequency EPR work on helix 8 of this channel-forming protein is in progress in Osnabrück and Berlin. For these experiments the necessary site-directed mutants of colicin A have been prepared in Marseille.

We conclude by stating that the presented multifrequency EPR work on colicin A mutants provides new insights into the molecular mechanisms of protein refolding for the formation of membrane channels by means of water-soluble protein complexes, such as bacterial toxins. The detailed information obtained is complementary to that of protein X-ray crystal-

lography, solid-state NMR, and optical spectroscopy techniques for determining the structure and dynamics of large biomolecules. High-field EPR, in particular, can provide additional information on transient intermediates of proteins in action, because they can be observed while staying in their working states on biologically relevant time scales. By extending 95 GHz high-field EPR to 360 GHz EPR, even the g_{yy} tensor component of the NO• labeled proteins can be resolved.[57] Thereby, an additional probe becomes available for measuring effects of the microenvironment on the structure and mobility of site-specifically spin labeled proteins at work.

Acknowledgment. We are thankful to Matthias Pfeiffer and Dieter Oesterhelt (MPI Martinsried) for providing the bacteriorhodopsin mutants and to Jack Freed (Cornell University) for stimulating discussions about high-field/high-frequency EPR. We gratefully acknowledge the support of the Deutsche Forschungsgemeinschaft (DFG) in the frame of the DFG Priority Program "High-field EPR" (SPP 1051).

References and Notes

(1) Lakey, J. H.; van der Groot, G. F.; Pattus, F. *Toxicology* **1994**, *87*, 85 and references therein.
(2) Cramer, W. A.; Heymann, J. B.; Schendel, S. L.; Deriy, B. N.; Cohen, F. S.; Elkins, P. A.; Stauffacher, C. V. *Annu. Rev. Biophys. Biomol. Struct.* **1995**, *24*, 611 and references therein.
(3) Stroud, R. M. *Curr. Opin. Struct. Biol.* **1995**, *5*, 514.
(4) Stroud, R. M.; Reiling, K.; Wiener, M.; Freymann, D. *Curr. Opin. Struct. Biol.* **1998**, *8*, 525.
(5) Oh, K. J.; Zhan, H.; Cui, C.; Hideg, K.; Collier, R. J.; Hubbell, W. L. *Science* **1996**, *273*, 810.
(6) Huynh, P. D.; Cui, C.; Zhan, H.; Oh, K. J.; Collier, R. J.; Finkelstein, A. *J. Gen. Physiol.* **1997**, *110*, 229.
(7) Lacy, D. B.; Stevens, R. C. *Curr. Opin. Struct. Biol.* **1998**, *8*, 778.
(8) Salwinski, L.; Hubbell, W. L. *Protein Sci.* **1999**, *8*, 562.
(9) Wiener, M.; Freymann, D.; Ghosht, P.; Stroud, R. M. *Nature* **1997**, *385*, 461.
(10) Dankert, J. R.; Uratani, Y.; Grabau, C.; Cramer, W. A.; Hermodson, M. *J. Biol. Chem.* **1982**, *257*, 3857.
(11) Nardi, A.; Slatin, S. L.; Baty, D.; Duché, D. *J. Mol. Biol.* **2001**, *307*, 1293.
(12) Parker, M. W.; Postma, J. P. M.; Pattus, F.; Tucker, A. D.; Tsernoglou, D. *J. Mol. Biol.* **1992**, *224*, 639.
(13) Kim, Y.; Valentine, K.; Opella, S. J.; Schendel, S. L.; Cramer, W. A. *Protein Sci.* **1998**, *7*, 342.
(14) Lambotte, S.; Jasperse, P.; Bechinger, B. *Biochemistry* **1998**, *37*, 16.
(15) Menikh, A.; Saleh, M. T.; Gariepy, J.; Boggs, J. M. *Biochemistry* **1997**, *36*, 15865.
(16) Lakey, J. H.; Duché, D.; González-Manas, J.-M.; Baty, D.; Pattus, F. *J. Mol. Biol.* **1993**, *230*, 1055.
(17) Todd, A. P.; Cong, J.; Levinthal, F.; Levinthal, C.; Hubbell, W. L. *Proteins* **1989**, *6*, 294.
(18) Shin, Y. K.; Levinthal, C.; Levinthal, F.; Hubbell, W. L. *Science* **1993**, *259*, 960.
(19) Duché, D.; Parker, M. W.; González-Manas, J.-M.; Pattus, F.; Baty, D. *J. Biol. Chem.* **1994**, *269*, 6332.
(20) Merrill, A. R.; Cramer, W. A. *Biochemistry* **1990**, *29*, 8529.
(21) Slatin, S. L.; Qiu, X. Q.; Jakes, K. S.; Finkelstein, A. *Nature* **1994**, *371*, 158.
(22) Qiu, X. Q.; Jakes, K. S.; Kienker, P. K.; Finkelstein, A.; Slatin, S. L. *J. Gen. Physiol.* **1996**, *107*, 313.
(23) Hubbell, W. L.; Mchaourab, H. S.; Altenbach, C.; Lietzow, M. A. *Structure* **1996**, *4*, 779.
(24) Hubbell, W. L.; Gross, A.; Langen, R.; Lietzow, M. A. *Curr. Opin. Struct. Biol.* **1998**, *8*, 649.
(25) Hubbell, W. L.; Cafiso, D. S.; Altenbach, C. *Nat. Struct. Biol.* **2000**, *7*, 735.
(26) Steinhoff, H.-J. *Frontiers Biosci.* **2002**, *7*, C 97.
(27) Freed, J. H. *Annu. Rev. Phys. Chem.* **2000**, *51*, 655.
(28) Möbius, K. *Chem. Soc. Rev.* **2000**, *29*, 129.
(29) Smirnov, A. I. *Electron Paramagn. Reson., Spec. Period. Rep.* **2002**, *18*, 109.
(30) Prisner, T.; Rohrer, M.; MacMillan, F. *Annu. Rev. Phys. Chem.* **2001**, *52*, 279.
(31) Steinhoff, H.-J.; Savitsky, A.; Wegener, C.; Pfeiffer, M.; Plato, M.; Möbius, K. *Biochim. Biophys. Acta* **2000**, *1457*, 253.
(32) Wegener, C.; Savitsky, A.; Pfeiffer, M.; Möbius, K.; Steinhoff, H.-J. *Appl. Magn. Reson.* **2001**, *21*, 441.
(33) Plato, M.; Steinhoff, H.-J.; Wegener, C.; Törring, J. T.; Savitsky, A.; Möbius, K. *Mol. Phys.* **2002**, *100*, 3711.
(34) Altenbach, C.; Marti, T.; Khorana, H. G.; Hubbell, W. L. *Science* **1990**, *248*, 1088.
(35) Farahbakhsh, Z. T.; Altenbach, C.; Hubbell, W. L. *Photochem. Photobiol.* **1992**, *56*, 1019.
(36) Altenbach, C.; Greenhalgh, D. A.; Khorana, H. G.; Hubbell, W. L. *Proc. Natl. Acad. Sci. U.S.A.* **1994**, *91*, 1667.
(37) Peiffer, M.; Rink, T.; Gerwert, K.; Oesterhelt, D.; Steinhoff, H.-J. *J. Mol. Biol.* **1999**, *287*, 163.
(38) Steinhoff, H.-J.; Pfeiffer, M.; Rink, T.; Burlon, O.; Kurz, M.; Riesle, J.; Heuberger, E.; Gerwert, K.; Oesterhelt, D. *Biophys. J.* **1999**, *76*, 2702.
(39) Brunden, K. R.; Uratani, Y.; Cramer, W. A. *J. Biol. Chem.* **1984**, *259*, 7682.
(40) Hubbell, W. L.; Froncisz, W.; Hyde, J. S. *Rev. Sci. Intrum.* **1987**, *58*, 1879.
(41) Lin, Y.; Nielsen, R.; Murray, D.; Hubbell, W. L.; Mailer, C.; Robinson, B. H.; Gelb, M. H. *Science* **1998**, *279*, 1925.
(42) Kühn, M. Ph.D. Thesis, Ruhr-University of Bochum, 2003.
(43) Prisner, T. F.; Rohrer, M.; Möbius, K. *Appl. Magn. Reson.* **1994**, *7*, 167.
(44) Möbius, K.; Savitsky, A.; Fuchs, M. *Biol. Magn. Reson.*, in press.
(45) Burghaus, O.; Rohrer, M.; Götzinger, T.; Plato, M.; Möbius, K. *Meas. Sci. Technol.* **1992**, *3*, 765.
(46) Mchaourab, H. S.; Lietzow, M. A.; Hideg, K.; Hubbell, W. L. *Biochemistry* **1996**, *35*, 7692.
(47) Steinhoff, H.-J.; Hubbell, W. L. *Biophys. J.* **1996**, *71*, 2201.
(48) Kawamura, T.; Matsunami, S.; Yonezawa, T. *Bull. Chem. Soc. Jpn.* **1967**, *40*, 1111.
(49) Griffith, O. H.; Dehlinger; P. J.; Van, S. P. *J. Membr. Biol.* **1974**, *15*, 159.
(50) Lebedev, Y. S.; Grinberg, O. Y.; Dubinsky, A. A.; Poluektov, O. G. In *Bioactive Spin Labels*; Zhadanov, J. I., Ed.; Springer-Verlag: Berlin, 1992; p 228.
(51) Earle, K. A.; Moscicki, J. K.; Ge, M.; Budil, D. E.; Freed, J. H. *Biophys. J.* **1994**, *66*, 1213.
(52) Gulla, A. F.; Budil, D. E. *J. Phys. Chem. B* **2001**, *105*, 8056.
(53) Ding, Z.; Gulla, A. F.; Budil, D. E. *J. Chem. Phys.* **2001**, *115*, 10685.
(54) Marsh, D.; Kurad, D.; Livshits, V. A. *Chem. Phys. Lipids* **2002**, *116*, 93.
(55) Tory, C.; Merrill, A. R. *J. Biol. Chem.* **1999**, *274*, 24539.
(56) Kienker, P. K.; Qiu, X.-Q.; Slatin, S. L.; Finkelstein, A.; Jakes, K. S. *J. Membr. Biol.* **1997**, *157*, 27.
(57) Fuchs, M.; Prisner, T. F.; Möbius, K. *Rev. Sci. Instrum.* **1999**, *70*, 3681.
(58) Subramaniam, S.; Henderson, R. *Nature* **2000**, *406*, 653.